Wideband Widebeam Circular-Polarized Antenna Using Asymmetrical Tri-Dipoles for Direct Satellite-to-Handset Communications

Peihang Li, Yongjian Zhang, *Member, IEEE*, Xu Qin, *Member, IEEE*, Kunpeng Wei, *Senior Member, IEEE*, Peiyu Liang, and Yue Li, *Senior Member, IEEE*

***Abstract*— This article presents a compact wideband circular-polarized (CP) antenna with wide beamwidth for low-orbit direct satellite-to-handset communication. In this design, an asymmetric tri-dipole antenna is proposed and integrated onto the upper bezel of mobile terminal. The contributions of the asymmetry are with three aspects: 1) the antenna is composed of asymmetrical dipoles to generate circular polarization, i.e., a folded dipole for horizontal polarization (HP) and two bent dipoles for vertical polarization (VP); 2) the two bent dipoles are also asymmetrical to improve both impedance and axial ratio (AR) bandwidths; and 3) for each bent dipole, the two arms are asymmetrically designed to enhance the beamwidth for low-orbit range coverage. To validate, a prototype of the proposed antenna was fabricated and tested, indicating gratifying circular polarization performance of −6-dB impedance bandwidth of 680 MHz, 3-dB AR bandwidth of 140 MHz, and 3-dB beamwidth beyond 92° in a volume of 0.88 × 0.07 × 0.005λ_0^3 at the center frequency of 3.8 GHz. With the merits of compact size, wide bandwidth, and wide beamwidth, this asymmetric tri-dipole CP antenna exhibits potential for mobile terminal applications of low-orbit satellite communications.**

***Index Terms*— Circular polarization, dipole antenna, feeding network, satellite communications, wideband antenna.**

I. Introduction

WIRELESS communications based on mobile terminals have already become an indispensable aspect of daily life. However, the signal transmission in most mobile terminals heavily leans upon on-land base station systems, which only cover 10% of the global area [1]. Consequently, it is a serious challenge to provide seamless communications in remote areas without base stations, such as mountains, oceans, and deserts. As a feasible solution, satellites can perform as a relay station, providing reliable links and expanding communication coverage. To avoid the Faraday effect in the Earth's ionosphere that switches the polarization state of linearly polarized electromagnetic waves [2], circular-polarized (CP) antennas are often adopted for direct satellite-to-handset communication due to their inherent insensitivity to the direction of the transmitting and receiving antennas. As shown in Fig. 1, the CP antennas in the mobile terminals are expected to have wide operating bandwidth for compatibility with different satellites and wide beamwidth for large coverage in low-orbit satellite communications. However, the limited space within mobile terminals poses a challenge to integrating antenna with such high performances [3], [4], particularly in the CP antennas.

Fig. 1. Typical scenarios in low-orbit satellite mobile phone communications.

Various structures are used to design CP antennas in mobile terminals. They can be mainly categorized into two types, i.e., perturbation and multiantenna methods. In the perturbation method, an antenna usually provides two orthogonal modes by a main radiator. The phase difference of these two radiation modes can be adjusted by etching slots [5], [6], [7], cutting corners [8], [9], or adding parasitic structures [10], and then, the CP wave is synthesized. For example, by cutting off two corners of a square patch, two orthogonal modes of a microstrip antenna can be separated with a phase difference, resulting in CP radiation [11], [12]. These antennas using perturbation method can only realize a high-quality CP performance at a single frequency, leading to a narrow axial ratio (AR) bandwidth. Multiantenna method is exciting multiple antennas with orthogonal polarizations by a specific

Manuscript received 20 March 2024; revised 1 June 2024; accepted 17 June 2024. Date of publication 3 July 2024; date of current version 9 August 2024. This work was supported in part by the National Natural Science Foundation of China under Grant 62022045 and Grant U22B2016, in part by the National Key Research and Development Program of China under Grant 2021YFA0716601, and in part by Xiaomi Communications Company, Ltd. *(Corresponding author: Yue Li.)*

Peihang Li, Yongjian Zhang, Xu Qin, and Yue Li are with the Department of Electronic Engineering, Beijing National Research Center for Information Science and Technology, Tsinghua University, Beijing 100084, China (e-mail: lyee@tsinghua.edu.cn).

Kunpeng Wei and Peiyu Liang are with Xiaomi Communications Company Ltd., Beijing 100085, China.

Color versions of one or more figures in this article are available at https://doi.org/10.1109/TAP.2024.3420086.

Digital Object Identifier 10.1109/TAP.2024.3420086

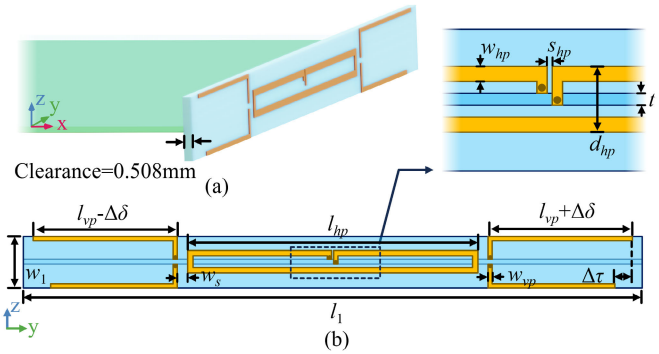

Fig. 2. Geometry of the proposed tri-dipole antenna on the upper bezel. (a) Isometric view. (b) Front view. $w_{hp} = 0.6$ mm, $s_{hp} = 0.2$ mm, $d_{hp} = 2.6$ mm, $l_{hp} = 33.8$ mm, $l_{vp} = 16.9$ mm, $w_{vp} = 0.4$ mm, $w_s = 1.3$ mm, $w_1 = 6$ mm, $l_1 = 74$ mm, $\Delta\delta = 0.2$ mm, and $\Delta\tau = 2$ mm.

feeding network. For instance, CP radiation is achieved by feeding regular-arranged inverted-F antennas [13], microstrip antennas [14], [15], [16], or antenna dipoles [17], [18], [19], [20] with sequential phases. Different antenna types can also be adopted for CP radiation generation, such as the combination of a dipole and a cavity in [21]. To reduce the occupying clearance, a compressed delay line is proposed in [22]. Besides, a dual-polarized magnetic dipole can be utilized with a wider AR bandwidth [23], [24], [25]. These multiantenna structures facilitate wider AR bandwidths [13], [21], [26], [27]. However, to align the radiation beam with the satellite, the antenna should be loaded in the upper bezel of the mobile terminals. The narrow bezel makes it impossible to load such a large-sized structure [11], [24], [28], [29]. Therefore, the CP antennas are difficult to directly apply to mobile terminals for satellite communications due to their narrow bandwidths or large volumes.

Here, a compact CP antenna with wide operating bandwidth and beamwidth is proposed and integrated onto the upper bezel of the mobile terminals for low-orbit satellite communications. The proposed antenna is constructed by an asymmetric tri-dipole structure. Specifically, a folded dipole is adopted in the middle area for horizontal polarization (HP), while two bent dipoles are employed on both sides for vertical polarization (VP). By artificially introducing asymmetries of this tri-dipole antenna, high performances, including wide AR bandwidth, wide impedance bandwidth, and wide beamwidth, are realized within a compact size of $0.47\lambda_0 \times 0.06\lambda_0 \times 0.004\lambda_0$ at the center frequency. The proposed antenna exhibits a compact size, wide bandwidth, and low clearance, making it suitable for direct satellite-to-handset communication.

II. Configuration and Desing of the Antenna

The structure of the proposed antenna is shown in Fig. 2. The whole antenna is integrated onto the upper bezel of the mobile terminal motherboard. The folded dipole in the center provides HP waves, while the bent vertical dipoles on both sides provide VP waves. The bent vertical dipoles on the left and right sides introduce an asymmetric parameter $\Delta\delta$, while the upper and lower arms of each vertical dipole introduce an asymmetric parameter $\Delta\tau$ to obtain better radiation characteristics. These three dipoles are fed through a microstrip line and a power splitter chip located on the motherboard. The substrate

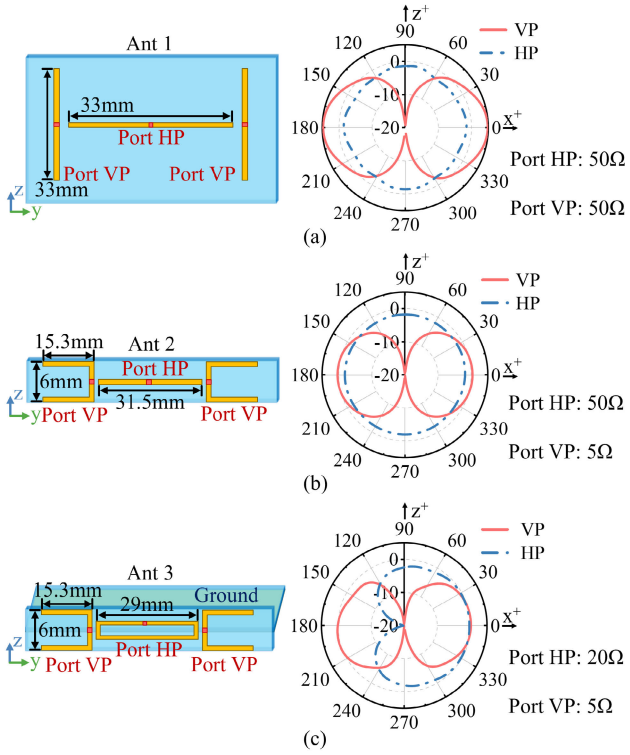

Fig. 3. Schematic of the structural evolution of the proposed antenna and radiation patterns in the *xoz* plane. (a) Conventional dipoles. (b) Bent dipoles with vertical compression. (c) Dipoles considering the ground of mobile terminal. The width of the dipole is set to 0.5 mm.

material is Rogers 5880 ($\varepsilon_r = 2.2$ and $\tan\delta = 0.0009$), and the thickness of the substrate is 0.508 mm. The backside of the motherboard is a copper plate, which is used to simulate the usage environment of the mobile terminal.

A. Antenna Evolution

To clearly demonstrate the working principle of the proposed antenna, its evolution process is provided here. For high-quality CP radiation, the far-field directivity of the horizontal and vertical polarized waves should be identical, while the phase difference between them should be equal to 90°. In addition, it is also valuable noting for the proposed tri-dipole scheme that the intrinsic impedance of three dipoles should be optimized to 150 Ω to match the three-way power splitter chip with the input port impedance of 50 Ω.

First, a conventional CP antenna based on three dipoles, named Ant. 1, is shown in Fig. 3(a). When the three ports with an intrinsic impedance of 50 Ω are excited with the power ratio of 1:1:1, the radiation pattern for the two polarizations can be obtained, as shown in Fig. 3(a). It can be observed that the directivity of the VP is 6 dB higher than one of the HP due to the binary array and twice the power ratio, resulting in quadruple VP wave directivity.

Then, to be compatible with the narrow upper bezel of the mobile terminals, the vertical dimensions of Ant. 1 should be compressed, leading to two bent VP dipoles shown as Ant. 2 in Fig. 3(b). The intrinsic impedance of the two VP dipoles decreases due to the cancellation of the horizontal currents generated by the upper and lower arms of the VP dipoles. When Ant. 2 is also matched and fed with the equal power

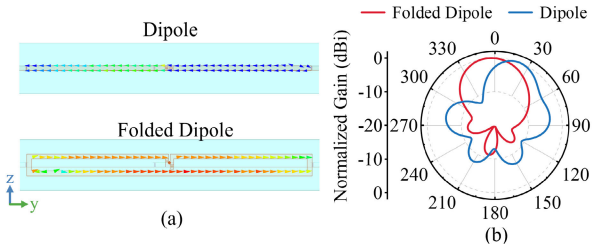

Fig. 4. (a) Current distribution of conventional dipole and folded dipole at center frequency. (b) Radiation pattern of conventional dipole and folded dipole at center frequency.

ratio, the radiation patterns of the VP and HP waves differ by ∼3 dB, which is not suitable for high-quality CP radiation.

Next, a horizontal metallic ground is introduced to simulate the mobile terminal usage environment, as shown in Fig. 3(c). Here, the conventional HP dipole in Ant. 2 is replaced by a folded dipole in Ant. 3 to mitigate the effects of reverse induced currents on the HP antenna and to achieve a more uniform current distribution. As shown in Fig. 4, when using an HP dipole, one arm is connected to the microstrip line, while the other arm is connected to the ground. This asymmetry causes an unbalanced current distribution along the dipole. For a folded dipole, the current distribution becomes balanced, as illustrated in Fig. 4(a). Accordingly, the radiation patterns of HP antenna with different configurations are depicted in Fig. 4(b). Here, the unbalanced current distribution in the conventional dipole distorts the main lobe of the radiation pattern, while the main lobe of the folded dipole points directly upward. The right side of Fig. 3(c) shows the radiation pattern of Ant. 3 when the port impedance is matched. The HP realized gain and VP realized gain of the antenna are comparable in the direction of the $+x$-axis. This means that the designed triple dipole structure can achieve high-quality CP radiation under the premise of impedance matching.

B. Feeding Technique

In addition to the antenna structure, the design of the antenna feeding circuit on the motherboard is worth considering because of the special environmental configurations of mobile terminals. Ant. 4 provides an initial design for the feeding method of Ant. 3, as depicted in Fig. 5(a), where the microstrip line is located on the motherboard and adopted to excite three dipoles. The green part represents the metal ground. The relevant parameters are set as follows: $w_2 = 1$ mm, $w_3 = 1$ mm, $w_6 = 2$ mm, $w_7 = 2.5$ mm, $l_2 = 2$ mm, and $l_3 = 1.5$ mm. The input ports of the three antennas, i.e., ports 1–3, are set at 150 Ω, considering that three antennas must be combined into one port. It can be seen in the result of S-parameters, as shown in Fig. 5(c) and (d), that three dipoles are not matched well.

To effectively excite the three antennas, Ant. 5 loads several components at the ports for matching, with capacitance and inductance values of 0.6 pF, 0.12 pF, and 4.5 nH, as shown in Fig. 5(b). The center frequency of the proposed antenna is successfully tuned around 3.8 GHz by the additional loaded components. It should be noted that the impedance bandwidth of the HP antenna is wider than that of the VP antenna, as shown in Fig. 5(c) and (d). If the HP and VP antennas are directly tuned to the same frequency, the AR bandwidth of the

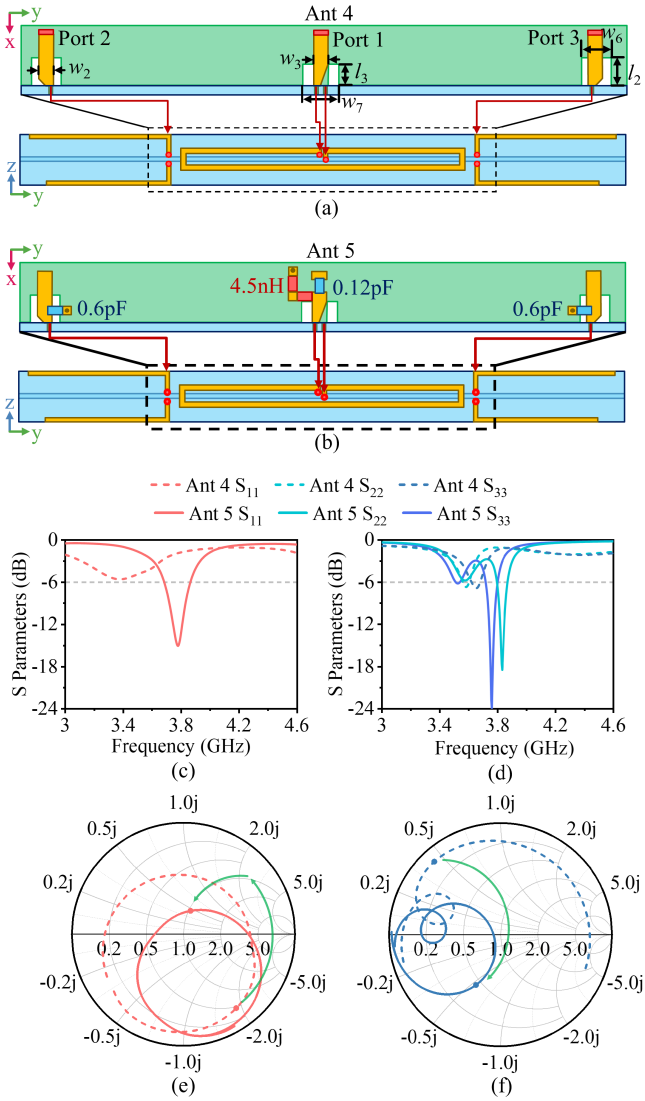

Fig. 5. Schematic of (a) Ant. 4 and (b) Ant. 5 with the corresponding impedance curves. (c) S-parameters of HP antenna (Port 1). (d) S-parameters of VP antennas (Ports 2 and 3). (e) Impedance on the Smith chart of the HP antenna (Port 1). (f) Impedance on the Smith chart of the VP antennas (Ports 2 and 3).

final CP antenna will be comparable to the VP's bandwidth, resulting in the relatively wider bandwidth of the HP antenna being wasted. The overall impedance bandwidths of the VP and HP are ensured to be similar by artificially introducing an asymmetry ($2\Delta\delta$) in the length of the VP dipoles on both sides. The center frequencies of the two VP antennas are intentionally staggered and a larger AR bandwidth can be obtained.

The notches etched onto the motherboard play an equally important role in the proposed design. The upper arm of the dipole is connected to the microstrip line, while the lower arm is connected directly to the ground. Due to the overcompressed dimensions, the lower arm of the dipole will form a huge conductor with the ground, causing the radiation pattern of the VP dipoles to become a bent monopole pattern instead of a dipole pattern. As shown in Fig. 6(b), when the motherboard is not etched with notches, an unbalanced current distribution will occur on the upper and lower arms of the VP dipoles.

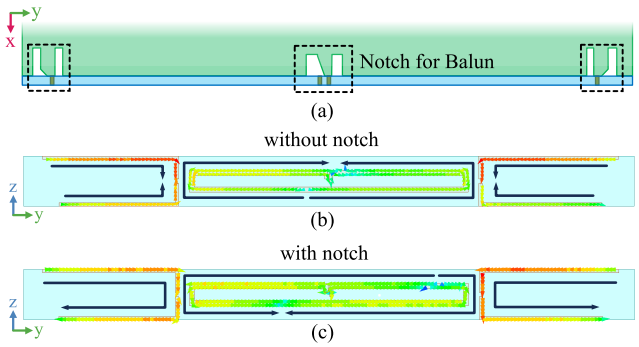

Fig. 6. Effect of notch on current distribution of Ant. 5. (a) Schematic of the notches. Current distribution of Ant. 5 (b) with notches and (c) without notches.

The upper and lower arms of the dipole have currents flowing in opposite directions and with different magnitudes. After etching notches, the current distribution of the upper and lower arms of the VP dipoles becomes balanced, as shown in Fig. 6(c). The dipole's upper and lower arms have currents flowing in the same direction, and the current distribution is more uniform. It means that the etching notches perform as a balun structure, leading to a quasi-standard dipole radiation pattern.

Apart from the matching process of the tri-dipole antenna, a high-quality CP wave should also require the specific phase of the two polarizations. In practice, the phase difference can be achieved by directly using mutual chips [27]. Since this work is mainly based on the idea of verification to design a prototype, the extra microstrip line is used here as a method to modify the phase in Ant. 6 shown as Fig. 7(a). As seen, a 90° phase difference can be achieved by using a microstrip line as a delay line. The relevant parameters of the delay line are set as $w_4 = 0.15$ mm, $w_5 = 0.45$ mm, $l_4 = 3.5$ mm, and $l_5 = 8$ mm. As the power splitter chip cannot be simulated in the commercial software, the proposed tri-dipole antenna is excited with equal power through the 150-Ω ports in the simulation section. The impedance curves of three ports are shown in Fig. 7(b), and the VP antenna achieves a comparable bandwidth to that of the HP antenna due to the asymmetric design. The gratifying AR bandwidth of 150 MHz can be achieved by adjusting the delay line, as shown in Fig. 7(c). The radiation pattern of the antenna is shown in Fig. 7(d) and (e), where the right-hand circular polarization beamwidths on both sides reach 118° and 92°. The main lobe is directed toward the satellite ($+x$-axis) with a broad beamwidth, contributing to low-orbit satellite communications.

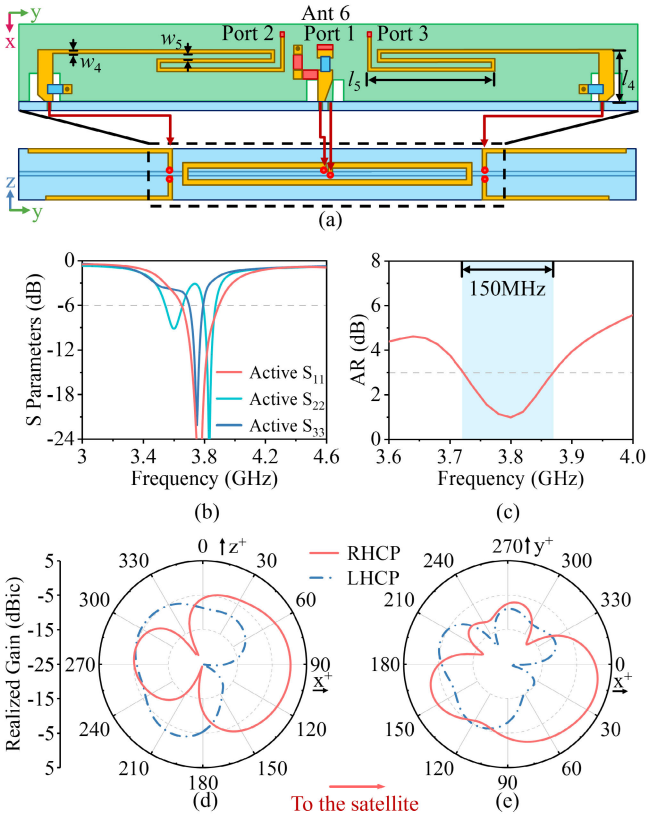

Fig. 7. Structure of Ant. 6 and the corresponding impedance state and far-field results. (a) Schematic of Ant. 6. (b) Active S-parameters for the three ports of Ant. 6. (c) AR of Ant. 6 around the center frequency. (d) Radiation patterns at 3.8 GHz of Ant. 6 in $\phi = 0°$ plane (xoz plane). (e) Radiation patterns at 3.8 GHz of Ant. 6 in $\theta = 90°$ plane (xoy plane).

C. Parametric Analysis

The proposed antenna introduces two parameters to regulate its asymmetry: $\Delta\tau$, which adjusts the variance between the upper and lower arms of the VP dipole, and $\Delta\delta$, which governs the length disparity between the left and right VP dipoles. The introduction of asymmetry directly influences the CP performance of the antenna.

For a single VP dipole, the difference in length between the upper and lower arms is represented as $\Delta\tau$. Besides the etching notch demonstrated in Fig. 6, the current distribution of the VP dipole can be further balanced by introducing the asymmetry $\Delta\tau$. The horizontal currents on the upper and lower arms of the VP dipole cannot be completely canceled by using the notches, which decay the main lobe and beamwidth. Fig. 8(b) shows the radiation patterns of the VP dipole at the center frequency with different $\Delta\tau$ values. The radiation pattern of the VP dipole points to the satellite direction ($+x$-axis) at $\Delta\tau = 2$ mm, while varying $\Delta\tau$ deteriorates the main lobe direction. On the other hand, the beamwidth of the VP antenna is also optimal at $\Delta\tau = 2$ mm, which is caused by the maximum cancellation of the horizontal current onto VP dipole, as shown in Fig. 8(c)–(e). The horizontal currents in the bent part are canceled completely, which reduces the effective radiation aperture of the VP dipoles. Accordingly, the directivity of the VP dipole decreases, and the designed antenna can achieve the maximum beamwidth [30]. It is worth noting that w_s can also impact the VP radiation performance. The spacing of the VP dipoles influences their array factor, consequently affecting the VP radiation gain.

The lengths of the left and right VP dipoles are also asymmetric described by the parameter $\Delta\delta$. Due to the wider impedance bandwidth of the HP dipole compared to that of the VP dipole, the combined CP bandwidth is relatively narrow. The center frequencies of the left and right VP dipoles can be adjusted to different bands by introducing $\Delta\delta$. Fig. 9 shows the far-field performance of the proposed antenna with

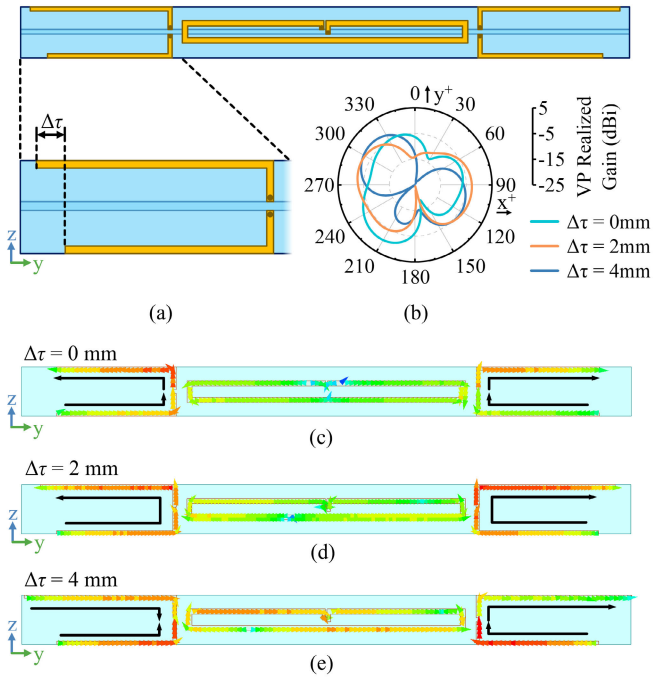

Fig. 8. Effect of the key parameter $\Delta\tau$ on the far-field performance of the proposed antenna. (a) Schematic of VP dipoles. (b) Vertical polarization radiation patterns of the proposed antenna at different $\Delta\tau$ conditions in $\theta = 0°$ plane (xoy plane). Current distribution of the proposed antenna when (c) $\Delta\tau = 0$ mm, (d) $\Delta\tau = 2$ mm and (e) $\Delta\tau = 4$ mm.

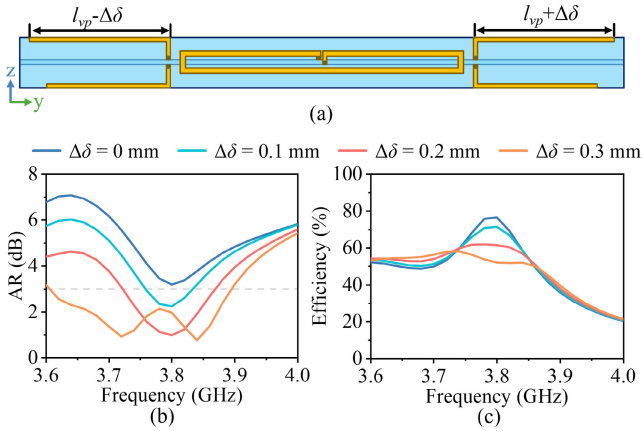

Fig. 9. Effect of the key parameter $\Delta\delta$ on the far-field performance of the proposed antenna. (a) Schematic of VP dipoles. (b) AR and (c) efficiency of the proposed antenna at different $\Delta\delta$ values.

different $\Delta\delta$ values. As $\Delta\delta$ increases, the AR bandwidth of the antenna becomes wider. Similarly, the center frequency gap between the two VP dipoles increases with the increment of $\Delta\delta$. The radiation from the VP antenna is distributed across a wide frequency range, ensuring that the proposed antenna maintains comparable HP and VP gains over a broad bandwidth. However, when $\Delta\delta$ is further increased, there is consistently one VP dipole operating at center frequency with poor efficiency or even mismatch. Consequently, the overall efficiency of the proposed antenna declines as $\Delta\delta$ increases, which is confirmed by Fig. 9(c). Therefore, $\Delta\delta = 0.2$ mm is ultimately selected as a compromise between AR broader bandwidth and maintaining efficiency.

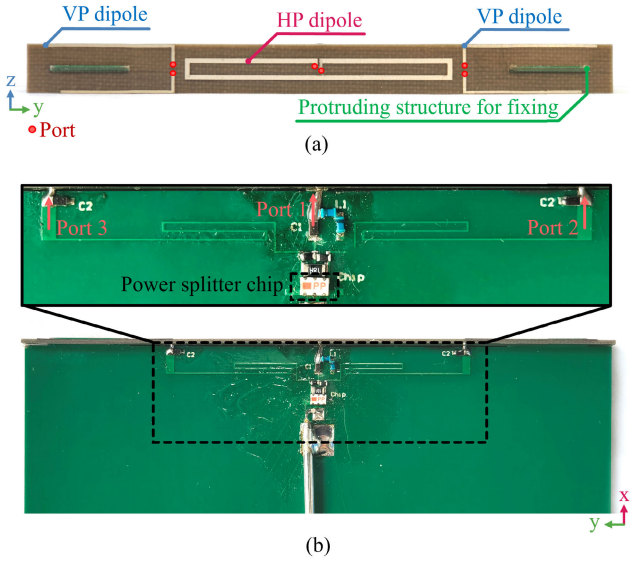

Fig. 10. Photographs of the proposed antenna prototype. (a) Radiating structure of the proposed antenna prototype. (b) Feed structure of the proposed antenna prototype.

III. Fabrication and Experimental Verification

To verify the feasibility of the simulation design, a prototype of the proposed tri-dipole antenna is fabricated, as shown in Fig. 10. The whole antenna is fed by a coaxial line, and the three dipole antennas are excited with a three-way power splitter chip. The chip model is SCG-3-392+. Fig. 10(a) shows the radiating structure of the antenna integrated onto the upper bezel of the mobile terminals. Two 0.508 × 10 mm rectangular slots were cut in the bezel, and a protruding rectangular structure was reserved in the motherboard for the assembly of the two parts. The motherboard size is set to 74 × 140 mm, and the proposed antenna is not sensitive to this dimension. Both the motherboard size and the battery positioned behind it have minimal impact on the antenna's radiation performance. The feeding circuit on the motherboard is depicted in Fig. 10(b) with the detailed structure in the insert figure.

Fig. 11(a) illustrates the final antenna structure with three 150-Ω resistors loaded in front of the chip, forming a compact power splitter structure with high isolation. To compensate for additional parasitic values inherent in the actual chip, two additional elements are loaded, as depicted in Fig. 11(b). The measured gain of the designed antenna is 2.42 dBic. The measured $|S_{11}|$ is shown in Fig. 11(c), revealing that the −6-dB bandwidth of the prepared antenna extends to 680 MHz. The additional bandwidth may be attributed to suboptimal power distribution within the power splitter chip. The AR bandwidths of the proposed antenna are shown in Fig. 11(d), and the −3-dB AR bandwidth near 3.8 GHz reaches 140 MHz (3.68%). The efficiency of the antenna near the center frequency is also within acceptable limits, as shown in Fig. 11(e). The efficiency of the antenna at 3.8 GHz is 67.5%. The results show good agreement between the actual prototype and the simulation.

The radiation patterns of the proposed antenna are depicted in Fig. 12, presenting both the measured and simulated results at three different frequencies. The main polarization (RHCP)

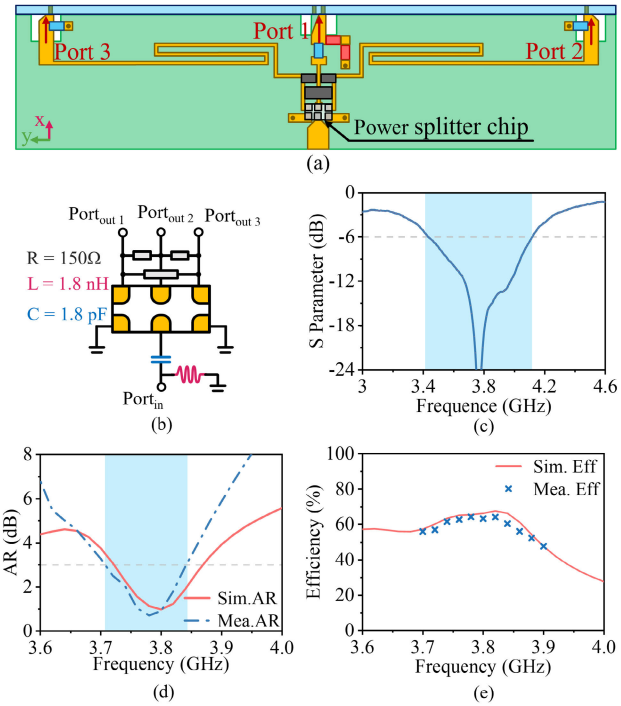

Fig. 11. Far-field performance of the proposed antenna. (a) Schematic of the proposed antenna prototype. (b) Circuit diagram of the power splitter chip and the external balance element. (c) Measured S-parameter curve of the proposed antenna. (d) Simulated and measured AR of the proposed antenna. (e) Simulated and measured efficiency of the proposed antenna.

TABLE I
COMPARISON FOR CP ANTENNAS

Ref.	Size (λ_0^2)	Clearance (mm)	Gain (dBic)	Beamwidth	Imp. BW	AR BW
[23]	0.14×0.14	15	4.75	104°/106°	4.7%	0.77%
[22]	0.60×0.32	8.8	3.99	168°/85°	6.2%	4.30%
[31]	0.39×0.38	6	3.80	92°/90°	9.6%	2.08%
[10]	0.46×0.06	0.5	4.80	94°/69°	10%	0.76%
T.W.	**0.88×0.07**	**0.5**	**2.42**	**112°/92°**	**17.8%**	**3.68%**

of the proposed antenna is toward the satellite ($+x$-axis). Notably, the proposed antenna exhibits a wide beamwidth, with measured half-power beamwidths reaching 112° (*xoz* plane) and 92° (*xoy* plane) at 3.8 GHz. This wide beamwidth enhances communication capability and facilitates calibration between the mobile terminal and the low-orbit satellite.

Table I summarizes the performance of the proposed antenna and other CP antennas. The impedance bandwidth is calculated with reference to −6 dB, which is a common criterion in mobile terminal antenna design. Therefore, the impedance bandwidth criterion in Table I uniformly uses −6 dB to ensure fairness of comparison across different antennas. It is evident that the proposed antenna offers a compact size and clearance while achieving satisfactory AR bandwidth performance. In contrast, the designs in [22], [23], and [31] demonstrate ideal circular polarization performance but necessitate redundant clearance makes it unsuitable for CP antenna design of mobile terminals. The antenna design presented in [31] is tailored for the practical application scenario of foldable mobile terminals. However, this design imposes additional constraints on the application, requiring the screen

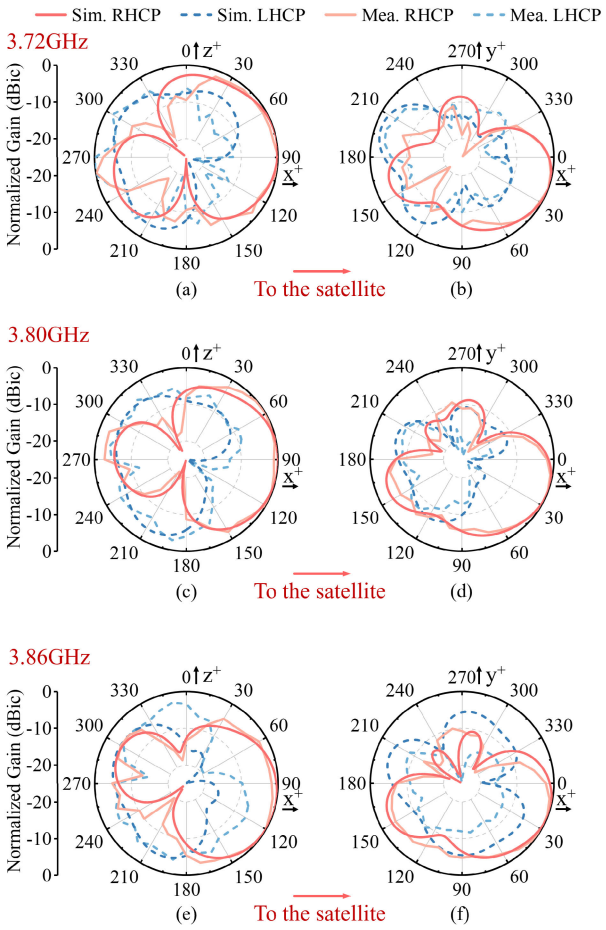

Fig. 12. Simulated and measured normalized radiation patterns at 3.72 GHz of the proposed antenna in (a) $\phi = 0°$ plane (*xoz* plane) and (b) $\theta = 0°$ plane (*xoy* plane). The patterns of the antenna at 3.80 GHz in (c) *xoz* plane and (d) *xoy* plane. The patterns of the antenna at 3.86 GHz in (e) *xoz* plane and (f) *xoy* plane.

to be folded by 90°. Cao et al. [10] exhibit superior CP performance and apply to mobile terminals. However, its design features high gain and narrow beamwidth, making it specifically tailored for high-orbit satellite communications. In contrast, this work performs better AR bandwidth, compact size, and clearance, along with a wider beamwidth. Consequently, it is better suited for low-orbit satellite communication scenarios.

It is worth noting that although [10] has a smaller size, the antenna proposed in this article has a wider beamwidth because the bent part of the VP dipole in Fig. 2(b) does not radiate externally. Although the size of the proposed antenna is larger, the effective radiation aperture of the antenna is smaller than [10], which in turn has a wider beamwidth [30]. Since the main topic of this article is to verify the antenna effect, in actual production, the cross-polarization phase difference can be adjusted by loading the elements and equivalently merged with the matching elements in Fig. 5(b) to further achieve the integration [27].

IV. CONCLUSION

In this article, a compact CP antenna with wide beamwidth and AR bandwidth is proposed for direct satellite-to-handset communication. The proposed antenna comprises a tri-dipole scheme with multidimensional asymmetries, including the

adopting different shapes of dipoles for the purpose of integration onto the upper bezel of a compact mobile terminal, utilizing different lengths of two VP dipoles to enhance the impedance bandwidth and AR bandwidth, and introducing different offset positions on two parts of each VP dipole to enhance the beamwidth of antenna. The tri-dipoles are fed by an integrated power splitter chip, and the measurement results demonstrate that the proposed antenna achieves an impedance bandwidth of 680 MHz and an AR bandwidth of 140 MHz at 3.8 GHz. Additionally, the antenna achieves 3-dB beamwidths of 112° and 92°, with a clearance of 0.508 mm and a size of $0.88 \times 0.07 \times 0.005\lambda_0^3$. With its compact size and wide AR bandwidth, the proposed antenna emerges as an ideal candidate for low-orbit direct satellite-to-handset communication.

REFERENCES

[1] ITU, *Measuring Digital Development: Facts and Figures 2023*, International Telecommunication Union, Geneva, Switzerland, 2023.

[2] B. K. Banerjea, "On the propagation of electromagnetic waves through the atmosphere," *Proc. Roy. Soc. London. A. Math. Phys. Sci.*, vol. 190, no. 1020, pp. 67–81, 1947.

[3] Y. Zhang and Y. Li, "Wideband microstrip antenna in small volume without using fundamental mode," *Electromagn. Sci.*, vol. 1, no. 2, pp. 1–6, Jun. 2023.

[4] Y. Zhang, Y. Li, W. Zhang, Z. Zhang, and Z. Feng, "Omnidirectional antenna diversity system for high-speed onboard communication," *Engineering*, vol. 11, pp. 72–79, Apr. 2022.

[5] N.-W. Liu, L. Zhu, Z.-X. Liu, M. Li, G. Fu, and Y. Liu, "A novel low-profile circularly polarized diversity patch antenna with extremely small spacing, reduced size, and low mutual coupling," *IEEE Trans. Antennas Propag.*, vol. 70, no. 1, pp. 135–144, Jan. 2022.

[6] C. Deng, Y. Li, Z. Zhang, G. Pan, and Z. Feng, "Dual-band circularly polarized rotated patch antenna with a parasitic circular patch loading," *IEEE Antennas Wireless Propag. Lett.*, vol. 12, pp. 492–495, 2013.

[7] J. Zeng, X. Liang, L. He, F. Guan, F. H. Lin, and J. Zi, "Single-fed triple-mode wideband circularly polarized microstrip antennas using characteristic mode analysis," *IEEE Trans. Antennas Propag.*, vol. 70, no. 2, pp. 846–855, Feb. 2022.

[8] K. Y. Lam, K.-M. Luk, K. F. Lee, H. Wong, and K. B. Ng, "Small circularly polarized U-slot wideband patch antenna," *IEEE Antennas Wireless Propag. Lett.*, vol. 10, pp. 87–90, 2011.

[9] Y. Dong et al., "Broadband circularly polarized filtering antennas," *IEEE Access*, vol. 6, pp. 76302–76312, 2018.

[10] Z. Cao, L. Chang, Y. Li, K. Wei, and Z. Zhang, "Compact mobile terminal antenna with endfire circularly polarized beam for satellite communications," *IEEE Trans. Antennas Propag.*, vol. 71, no. 12, pp. 9980–9985, Dec. 2023.

[11] M.-C. Tang, X. Chen, M. Li, and R. W. Ziolkowski, "A bandwidth-enhanced, compact, single-feed, low-profile, multilayered, circularly polarized patch antenna," *IEEE Antennas Wireless Propag. Lett.*, vol. 16, pp. 2258–2261, 2017.

[12] S. Ye, J. Geng, X. Liang, Y. J. Guo, and R. Jin, "A compact dual-band orthogonal circularly polarized antenna array with disparate elements," *IEEE Trans. Antennas Propag.*, vol. 63, no. 4, pp. 1359–1364, Apr. 2015.

[13] M.-S. Wang, X.-Q. Zhu, Y.-X. Guo, and W. Wu, "Miniaturized dual-band circularly polarized quadruple inverted-F antenna for GPS applications," *IEEE Antennas Wireless Propag. Lett.*, vol. 17, no. 6, pp. 1109–1113, Jun. 2018.

[14] Y. Zhang, Y. Li, M. Hu, P. Wu, and H. Wang, "Dual-band circular-polarized microstrip antenna for ultrawideband positioning in smartphones with flexible liquid crystal polymer process," *IEEE Trans. Antennas Propag.*, vol. 71, no. 4, pp. 3155–3163, Apr. 2023.

[15] C. Deng, Y. Li, Z. Zhang, and Z. Feng, "A wideband sequential-phase fed circularly polarized patch array," *IEEE Trans. Antennas Propag.*, vol. 62, no. 7, pp. 3890–3893, Jul. 2014.

[16] Y. Li, Z. Zhang, and Z. Feng, "A sequential-phase feed using a circularly polarized shorted loop structure," *IEEE Trans. Antennas Propag.*, vol. 61, no. 3, pp. 1443–1447, Mar. 2013.

[17] H. H. Tran, I. Park, and T. K. Nguyen, "Circularly polarized bandwidth-enhanced crossed dipole antenna with a simple single parasitic element," *IEEE Antennas Wireless Propag. Lett.*, vol. 16, pp. 1776–1779, 2017.

[18] J. Baik, T. Lee, S. Pyo, S. Han, J. Jeong, and Y. Kim, "Broadband circularly polarized crossed dipole with parasitic loop resonators and its arrays," *IEEE Trans. Antennas Propag.*, vol. 59, no. 1, pp. 80–88, Jan. 2011.

[19] T. K. Nguyen, H. H. Tran, and N. Nguyen-Trong, "A wideband dual-cavity-backed circularly polarized crossed dipole antenna," *IEEE Antennas Wireless Propag. Lett.*, vol. 16, pp. 3135–3138, 2017.

[20] Y. He, W. He, and H. Wong, "A wideband circularly polarized cross-dipole antenna," *IEEE Antennas Wireless Propag. Lett.*, vol. 13, pp. 67–70, 2014.

[21] W.-H. Zhang, W.-J. Lu, and K.-W. Tam, "A planar end-fire circularly polarized complementary antenna with beam in parallel with its plane," *IEEE Trans. Antennas Propag.*, vol. 64, no. 3, pp. 1146–1152, Mar. 2016.

[22] M. Ye, X. Li, and Q. Chu, "Single-layer circularly polarized antenna with fan-beam endfire radiation," *IEEE Antennas Wireless Propag. Lett.*, vol. 16, pp. 20–23, 2017.

[23] Z. Wang, S. Liu, and Y. Dong, "Electrically small, low-Q, wide beam-width, circularly polarized, hybrid magnetic dipole antenna for RFID application," *IEEE Trans. Antennas Propag.*, vol. 69, no. 10, pp. 6284–6293, Oct. 2021.

[24] S. Liu, Z. Wang, and Y. Dong, "Electrically small circularly polarized antenna based on capacitively loaded loop," *IEEE Antennas Wireless Propag. Lett.*, vol. 21, no. 9, pp. 1767–1771, Sep. 2022.

[25] Z. Wang, Y. Dong, Y. Ning, and T. Itoh, "Miniaturized circularly polarized periodically structured surface antenna for RFID application inspired by SRR," *IEEE Trans. Antennas Propag.*, vol. 69, no. 11, pp. 7269–7277, Nov. 2021.

[26] M. Hu, Y. Li, Y. Zhang, P. Wu, and H. Wang, "Ultrathin dual-band circularly polarized antenna," *IEEE Antennas Wireless Propag. Lett.*, vol. 23, no. 3, pp. 930–934, Mar. 2024.

[27] Y. Zhang and Y. Li, "Wideband isotropic antenna with miniaturized ground for enhanced 3 dB coverage ratio," *IEEE Antennas Wireless Propag. Lett.*, vol. 21, no. 6, pp. 1253–1257, Jun. 2022.

[28] H. Yang, Y. Fan, and X. Liu, "A compact dual-band stacked patch antenna with dual circular polarizations for BeiDou navigation satellite systems," *IEEE Antennas Wireless Propag. Lett.*, vol. 18, no. 7, pp. 1472–1476, Jul. 2019.

[29] L. Wen et al., "Compact and wideband crossed dipole antenna using coupling stub for circular polarization," *IEEE Trans. Antennas Propag.*, vol. 70, no. 1, pp. 27–34, Jan. 2022.

[30] H. Li, Z. Zhou, Y. Zhao, and Y. Li, "Low-loss beam synthesizing network based on epsilon-near-zero (ENZ) medium for on-chip antenna array," *Chip*, vol. 2, no. 2, Jun. 2023, Art. no. 100049.

[31] X. Zhang, K. Wei, Y. Li, and Z. Zhang, "A polarization reconfigurable antenna for satellite communication in foldable smartphone," *IEEE Trans. Antennas Propag.*, vol. 71, no. 12, pp. 9938–9943, Dec. 2023.

Peihang Li received the B.S. degree from Shanxi University, Taiyuan, China, in 2020, and the M.S. degree from the University of Electronic Science and Technology of China, Chengdu, China, in 2023, where he is currently pursuing the Ph.D. degree in electronic engineering.

His current research interests include terminal antennas, metamaterial antennas, and epsilon-near-zero antennas.

Yongjian Zhang (Member, IEEE) received the B.S. degree in communication engineering from Tongji University, Shanghai, China, in 2018, and the Ph.D. degree in electronic engineering from Tsinghua University, Beijing, China, in 2023.

He is currently a Post-Doctoral Fellow with the Department of Electronic Engineering, Tsinghua University. His current research interests include aircraft antennas, dual-polarized antennas, and multiple-input and multiple-output (MIMO) antenna arrays.

Dr. Zhang serves as a reviewer for the IEEE TRANSACTIONS ON ANTENNAS AND PROPAGATION, IEEE ANTENNAS AND WIRELESS PROPAGATION LETTERS, and *Microwave and Optical Technology Letters*.

Xu Qin (Member, IEEE) received the B.S. degree in electronic engineering from Tsinghua University, Beijing, China, in 2019, where he is currently pursuing the Ph.D. degree in electronic engineering.

His research interests include metamaterials, small antenna, and microstrip antenna.

Kunpeng Wei (Senior Member, IEEE) received the B.S. degree in electronic and information engineering from Huazhong University of Science and Technology, Wuhan, China, in 2008, and the Ph.D. degree in electrical engineering from Tsinghua University, Beijing, China, in 2013.

From July 2013 to December 2015, he was employed with the Radar Research Institute of Chinese Air Force Research Laboratory, Beijing, conducting research in the areas of phased-array antenna design and radar system design. He joined Consume Business Group of Huawei Inc., Xi'an, China, in 2016, where he had been an Antenna Specialist and the Director of Xi'an Antenna Team for five years. In 2021, he joined Honor Device Company Ltd., Beijing, when this company split from Huawei and he was the Director of Honor Antenna Team. After leaving Honor, he joined Xiaomi Corporation, Beijing, in 2023. He is currently the Chief Antenna Expert and the Head of the Antenna Technology Team. He leads a large group of antenna experts and engineers and takes the full responsibility in the research of antenna technologies to guarantee the market success of all Xiaomi's products ranging from smartphones, electric cars, tablets, laptops, and other IOT devices. He is a special level external expert of China Academy of Information and Communications Technology. He is also an Adjunct Professor with the School of Electronics and information engineering, Shenzhen University, Shenzhen, China. He has authored over referred 50 articles on consumer electronics antenna design. He holds over 50 granted U.S./EU/JP/CN patents and has other more than 20 patent applications in pending. His current research interests include meta-antennas, smart-phone antenna design, small size 5G antenna systems in terminal device, and millimeter-wave antenna array.

Dr. Wei is an IET Fellow. He was a recipient of the Principal Scholarship of Tsinghua University in 2012, the Huawei Team Gold Medal Award in 2017, the Huawei Individual Gold Medal Award in 2018, and the Honor Team Gold Medal Award in 2021. He has been serving as an Associate Editor for *IET Electronics Letters* since October 2021 and IEEE OPEN JOURNAL OF ANTENNAS AND PROPAGATION since October 2023.

Peiyu Liang received the B.S. and M.S. degrees from Beihang University, Beijing, China, in 2015 and 2018, respectively.

From 2016 to 2017, he was an Academic Guest with the Institute of Electromagnetic Theory, Technical University of Hamburg-Harburg, Hamburg, Germany. In 2018, he joined Xiaomi Corporation, Beijing, and he is currently a Senior Engineer specializing in smart-phone antennas. His research interests include circularly polarized antenna design for direct communication between mobile phones and satellites and characteristic mode analysis of mutual coupling between antennas and wireless.

Yue Li (Senior Member, IEEE) received the B.S. degree in telecommunication engineering from Zhejiang University, Hangzhou, Zhejiang, China, in 2007, and the Ph.D. degree in electronic engineering from Tsinghua University, Beijing, China, in 2012.

In June 2012, he was a Post-Doctoral Fellow with the Department of Electronic Engineering, Tsinghua University. In December 2013, he was a Research Scholar with the Department of Electrical and Systems Engineering, University of Pennsylvania, Philadelphia, PA, USA. He was also a Visiting Scholar with the Institute for Infocomm Research (I2R), A∗STAR, Singapore, in 2010, and the Hawaii Center of Advanced Communication (HCAC), University of Hawaii at Manoa, Honolulu, HI, USA, in 2012. Since January 2016, he has been with Tsinghua University, where he is currently an Assistant Professor and an Associate Professor with the Department of Electronic Engineering. He has authored and co-authored over 210 journal articles and 50 international conference papers. He holds 26 granted Chinese patents. His current research interests include metamaterials, plasmonics, electromagnetics, nanocircuits, mobile and handset antennas, MIMO and diversity antennas, and millimeter-wave antennas and arrays.

Dr. Li was a recipient of the URSI General Assembly and Scientific Symposium (GASS) in 2014, the Asia–Pacific Radio Science Conference (AP-RASC) in 2016, the International Symposium on Electromagnetic Theory (EMTS) in 2016, the Issac Koga Gold Medal from URSI General Assembly in 2017, the Second Prize of Science and Technology Award of China Institute of Communications in 2017, the International Applied Computational Electromagnetics Society Symposium (ACES) in 2018, the Atlantic Radio Science Conference (AT-RASC) in 2018, and the Young Scientist Award from the Conferences of Progress in Electromagnetics Research Symposium (PIERS) in 2019. He is serving as an Associate Editor for IEEE TRANSACTIONS ON ANTENNAS AND PROPAGATION, IEEE ANTENNAS AND WIRELESS PROPAGATION LETTERS, *Microwave and Optical Technology Letters*, and *Computer Applications in Engineering Education*. He is also serving on the Editorial Board of *Scientific Reports*, *Sensors*, and *Electronics*.